INSTITUTE OF PHYSICS PUBLISHING MEASUREMENT SCIENCE AND TECHNOLOGY
Meas. Sci. Technol. **14** (2003) 1998–2005 PII: S0957-0233(03)61892-8

Interrogation of free-space Fabry–Perot sensing interferometers by angle tuning

P C Beard

Department of Medical Physics and Bioengineering, University College London, Shropshire House, 11-20 Capper Street, London WC1E 6JA, UK

Received 8 April 2003, in final form 4 August 2003, accepted for publication 8 August 2003
Published 19 September 2003
Online at stacks.iop.org/MST/14/1998

Abstract
A method of interrogating a free-space Fabry–Perot sensing interferometer (FPI) by angle tuning the incident beam in order to vary the optical pathlength is described. A system based on a PC controlled precision galvanometer and a 1–1 beam expander that enabled the angle of incidence to be rapidly and continuously varied without translation is described. This system was used to demonstrate that the transfer functions (ITF) of low finesse FPIs of optical thicknesses in the range 80–200 μm could be accurately recovered by tuning the angle of incidence over less than 9°. Two sensor interrogation schemes are described. One involves scanning through the ITF in constant phase steps by applying an arcosine voltage waveform to the galvanometer and then returning to the angle at which the ITF phase derivative is a maximum. The other uses a mirror continuously rotating through 360° to repetitively scan through the ITF in constant angular steps. The signal is then recovered at the instant in time that the maximum value of the ITF derivative occurs. It is considered that angle tuning offers a flexible and inexpensive alternative to interrogating free-space FP sensors by wavelength tuning.

Keywords: Fabry–Perot, sensing, interrogation, angle tuning, ultrasound

1. Introduction

Fabry–Perot (FP) sensing interferometers have been used to detect a variety of measurands among them strain [1], temperature [2] and acoustic waves [3–5]. The transduction mechanism is one in which a time varying external measurand acts upon the FP cavity to linearly alter its optical pathlength. This produces an optical phase shift $\mathrm{d}\phi(t)$ which, via the intensity-phase transfer function (ITF) $I_R(\phi)$ of the interferometer, the characteristic periodic function that describes the shape of the reflected interference fringes, is converted to a corresponding reflected intensity modulation. If $\mathrm{d}\phi(t)$ is sufficiently small, it can be regarded as acting around a static phase bias or working point ϕ_o as depicted in figure 1. The FPI reflected intensity output can then be expressed in terms of the ITF as

$$I_R(\phi_o + \mathrm{d}\phi(t)) = I_R(\phi_o) + I'_R(\phi_o)\,\mathrm{d}\phi(t) \qquad (1)$$

where $I_R(\phi_o)$ is the static phase bias term defined by the laser wavelength and optical pathlength in the absence of a measurand and $I'_R(\phi_o)\,\mathrm{d}\phi(t)$ is the time varying signal term that is linearly dependent upon the measurand. $I'_R(\phi_o)$ is the phase derivative of the transfer function at ϕ_o and represents the sensitivity of the sensor to a measurand-induced phase shift—it is termed the phase sensitivity.

A difficulty is that the transfer function is inherently nonlinear (e.g. a raised cosine for a low finesse FPI as shown in figure 1). The phase sensitivity and hence the signal term are therefore dependent upon ϕ_o which may vary due to changes in cavity optical thickness and laser wavelength.

The situation is illustrated in figure 2. Figure 2(a) shows the reflected interference fringe distribution from a free-space 40 μm thick polymer film FP interferometer. This was obtained by scanning a normally incident, focused He–Ne laser beam over the FPI surface, detecting the reflected intensity (the phase bias term in equation (1)) using a photodiode and recording its dc voltage output V_{dc} for each point of the scan [6]. The variations in intensity in figure 2(a) are due to phase bias variations arising from changes in optical

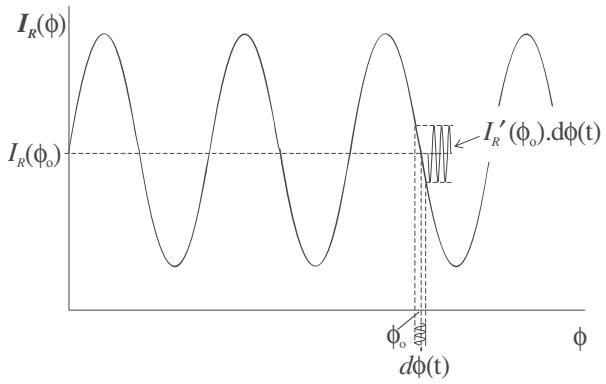

Figure 1. Operation of a low finesse FP sensing interferometer.

thickness across the polymer film. Simultaneously, to create a signal term, the output of a pulsed 3.5 MHz PZT ultrasound transducer (coupled via a water layer) was directed on to the FPI thereby modulating its optical thickness and producing a small (<150 mrad) time varying phase shift $d\phi(t)$. The photodiode output dv_{ac} due to the resulting reflected intensity modulation (the signal term in equation (1)) was high pass filtered to separate it from V_{dc} and its amplitude plotted a function of position as shown in figure 2(b). Assuming that the acoustically-induced phase shift was constant, figure 2(b) can be regarded as a relative phase sensitivity map. This shows two curved contours of uniform sensitivity surrounded by largely insensitive regions. An obvious difficulty exists if it is required to address points on the sensor outside these contours, perhaps in order to map the spatial distribution of a measurand or, if making a measurement at a single point, the contours shift due to environmentally induced changes in FP cavity optical thickness or laser wavelength.

In order to control the position of the sensitivity contours and interrogate any point on the sensor, some method of remotely and continuously adjusting the phase bias over at least 2π radians is required. This could be achieved by tuning the laser wavelength over the free spectral range of the FP sensing cavity. Visible and NIR edge emitting laser diodes can be continuously wavelength tuned by modulating the injection current. However, their low current tuning coefficient (<0.01 nm mA^{-1}) limits their tuning range to approximately 0.5 nm and therefore the minimum FP cavity length ($\sim$0.5 mm) that can be addressed. Temperature tuning can provide a greater tuning range (typically several nanometres) but is slow. External cavity laser systems can provide the necessary continuous tuning range (>10 nm) to interrogate short cavity lengths, down to a few tens of microns [2], but are expensive. Limited output power (<20 mW) of external cavity laser systems can also present a limitation for certain applications—for example those that require illuminating a large area of the FPI with high intensity in order to map the 2D spatial distribution of a measurand [5, 9, 10].

In this paper, we describe an alternative method of remotely and continuously controlling the phase bias of free-space FPIs by tuning the angle of incidence of the illuminating beam. This approach has several advantages over wavelength tuning. Firstly, relatively large phase shifts can readily be produced by angle tuning, enabling short FPI cavity thicknesses ($\sim$50 μm) to be interrogated. Secondly, by not requiring a tunable laser, the source requirements are substantially relaxed, enabling almost any fixed wavelength laser source of sufficient coherence to be employed. So, for applications where cost is an issue, inexpensive He–Ne lasers or laser diodes can be used. For applications that require illuminating with high intensity, readily available high power laser diodes can be employed.

The use of an automatic angle-tuned phase bias control system to set the operating point of a FP polymer film ultrasound imaging sensor has been described in brief in [9]. A simple manually controlled method of angle tuning has also been used to optimize the sensitivity of a dielectric coated acoustic sensor for making point measurements [7]. In this paper, a more detailed description of the theory, practical implementation and experimental validation of angle tuning for FPI sensing is provided. In section 2 the relationship between incident angle and phase is described. Sections 3 and 4 describe the details of a practical angle-tuned phase bias control system and its experimental evaluation using low finesse reference FPIs. Section 5 discusses two practical sensor interrogation approaches.

2. Phase–angle relationship

The relationship between the phase ϕ and the angle θ of the incident light is established by considering the geometry of a plane parallel FP cavity illuminated by a collimated beam as illustrated in figure 3. Consider the two parallel rays p and q incident at angle θ. p is transmitted into the cavity and reflected from the rear mirror arriving at C. Here it superposes and interferes with the reflection of q from the front mirror. The resulting optical phase shift ϕ between the two reflections is given by

$$\phi(\theta) = \frac{2\pi}{\lambda}(\mathrm{OPD}) \tag{2}$$

where OPD is the difference in optical path lengths from points of equal phase, A and D on the two rays p and q respectively, to point C where they interfere:

$$\mathrm{OPD} = n_2\mathrm{ABC} - n_1\mathrm{DC} \tag{3}$$

where n_2 and n_1 are the refractive indices of the internal and external cavity media respectively. By simple geometry,

$$\mathrm{OPD} = n_2\left(\frac{2l}{\cos\theta'}\right) - 2ln_1\tan\theta'\sin\theta \tag{4}$$

where θ' is the internal cavity angle and l the separation of the reflecting surfaces. Using $n_1\sin\theta = n_2\sin\theta'$ to obtain an expression for the OPD in terms of the internal angle θ' gives

$$\mathrm{OPD} = 2n_2l\cos\theta'. \tag{5}$$

The phase shift in terms of θ' is then obtained by inserting equation (5) into (2) and, assuming the small angle approximation ($\theta' = n_1\theta/n_2$), can be written

$$\phi(\theta) = \frac{4\pi n_2 l}{\lambda}\cos\left(\frac{n_1}{n_2}\theta\right). \tag{6}$$

So, for example, a 100 μm thick FPI of refractive index $n_2 = 1.5$ in air and illuminated with 633 nm laser light, initially at normal incidence, would require a modest change in the angle of incidence of the illuminating beam of 5.6° to produce a 2π phase shift.

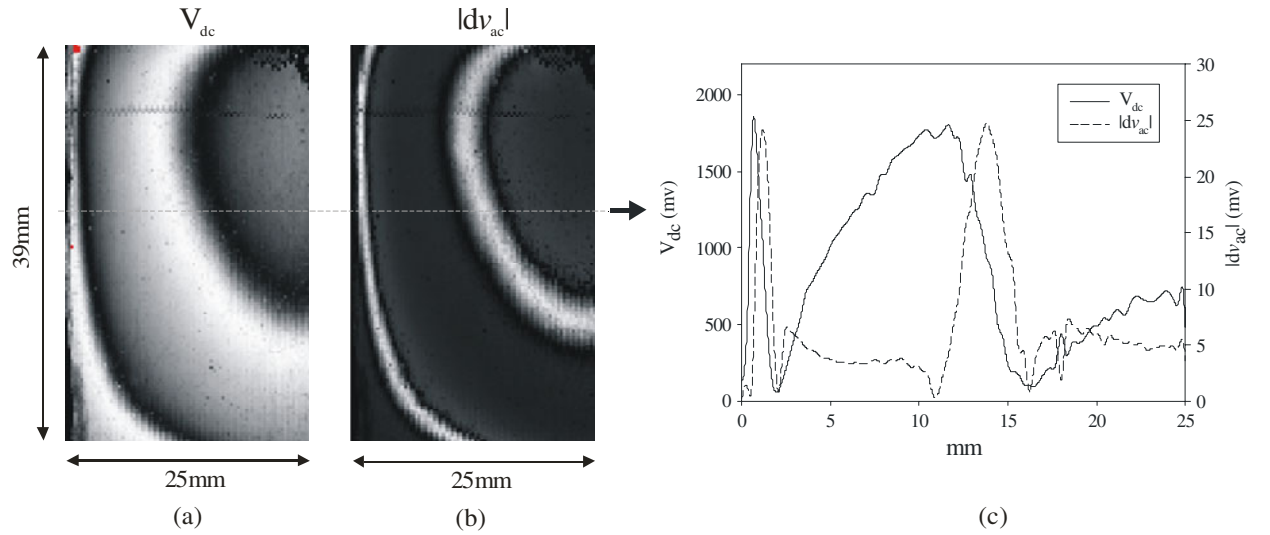

Figure 2. (a) Reflected dc intensity distribution from a 40 μm Fabry–Perot polymer film sensing interferometer (FPI) and (b) corresponding relative phase sensitivity map. (c) Horizontal profiles through (a) and (b) showing the minima of $|dv_{ac}|$ coinciding with the maxima and mimina of V_{dc}. The FPI was fabricated by vacuum depositing a 40 μm thick Parylene C polymer layer on to a semi-reflective aluminium coated glass substrate followed by a deposition of a highly reflective aluminium coating on to the polymer film [6]. The absorption in the aluminium coatings account for the asymmetric shape of the fringes [8] in (a).

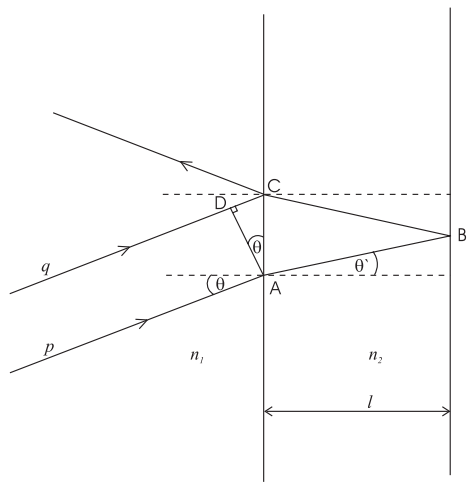

Figure 3. Ray construction for a plane parallel FP interferometer illuminated by a collimated beam of incidence angle θ.

3. Implementation—optical system

In order to vary ϕ by adjusting θ, an optical system that allows a collimated beam to be pivoted about its point of incidence on the FPI is required. Such a system is shown in figure 4. It employs a 1–1 beam expander arrangement comprising lenses L1 and L2 with a precision galvanometer mirror under PC control situated in the rear focal plane of L1. The FPI is positioned in the front focal plane (P1) of L2 and the reflected output beam equivalently reversed through the system by directing it through L3 and on to a photodiode of aperture 0.4 mm situated in focal plane (P2) of L3. All three lenses have the same focal length and diameter of 59 and 25 mm respectively. Changing the angle θ_{in} of the input beam using the galvanometer mirror produces a corresponding change in the angle θ of the light incident on the FP sensor without translating it across the surface. The light reflected from the sensor is directed on to the photodiode, also without translation, as θ_{in} is varied thus preserving the spatial correspondence between the sensor interrogation point in the plane P1 and its corresponding optical detection point at P2. By adjusting θ_{in}, and hence the optical pathlength of the interferometer, the contours of uniform sensitivity such as those shown in figure 2(b) can be scanned across the illuminated region of the sensor enabling any part of it to be interrogated with optimum sensitivity.

4. System evaluation

It is assumed that a change in the system input angle θ_{in} produces an identical change in θ and therefore a phase shift in accordance with equation (6). It is important to establish the validity of this assumption as in certain sensor interrogation schemes, such as that described in section 5.1, accurate recovery of the ITF is required to optimally set the working point of the FPI. Such schemes will be compromised if the ITF is distorted due to nondeterministic angle dependent changes in the relationship between phase and angle. This could be due to angular distortion in the optical system due, for example, to aberrations introduced by the lenses L1–3 such that $\theta \neq \theta_{in}$. Additionally, the ITF can become distorted if any of the optical components of the system possess significant angle dependent transmission characteristics due, e.g., to surface imperfections or anti-reflection coatings.

To investigate the significance of these effects and the validity of equation (6), comparisons were made between the measured and theoretical angle tuned ITFs of low finesse FPIs.

A glass cover slip of nominal thickness 150 μm was used as the FPI and positioned at P1 in figure 4. The Fresnel reflections (∼4%) due to the refractive index mismatches at the glass/air interfaces formed the mirrors of the interferometer. The mirror reflectivities are sufficiently low that the contribution of multiple intracavity reflections can be neglected and the system can be regarded as one of

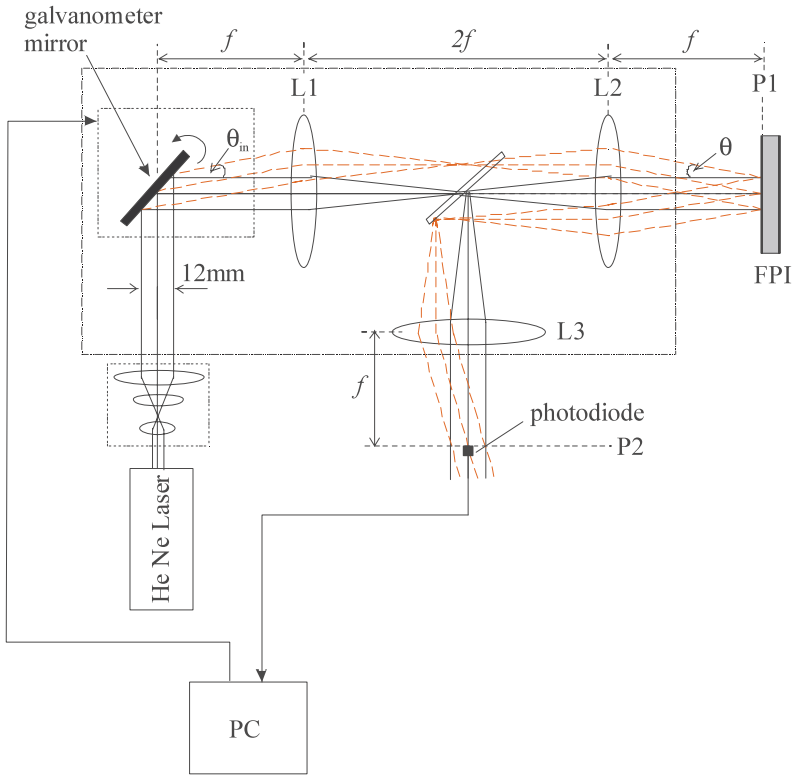

Figure 4. PC controlled angle tuning system. The galvanometer mirror is rotated to produce input angle θ_{in} resulting in a corresponding change in the output angle θ of the beam at P1 without translation. The reflected beam from the FPI is equivalently reversed through L3 so that there is also no translation of the beam at P2. The focal length f of lenses L1–3 is 59 mm.

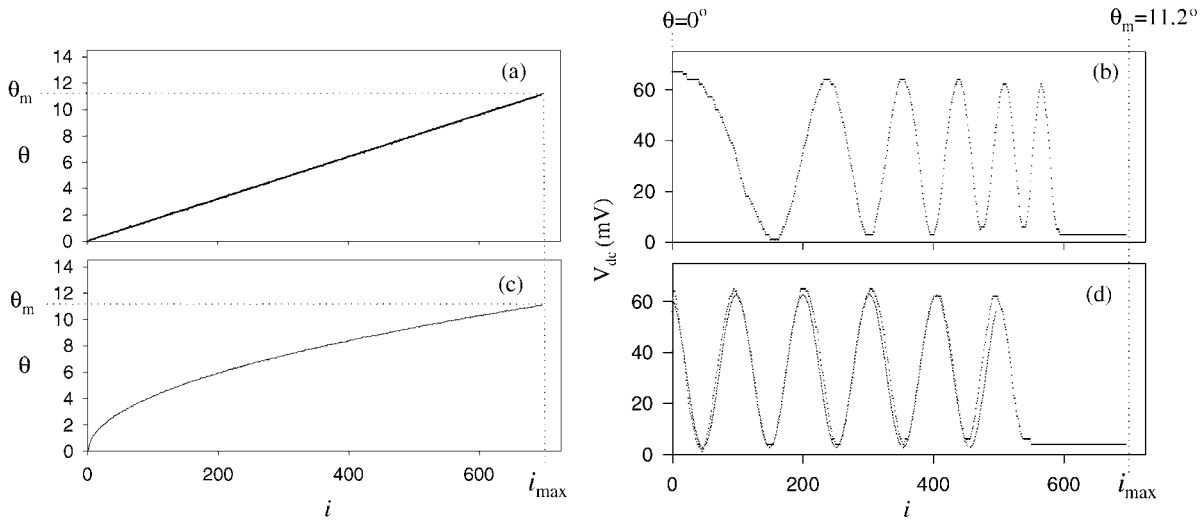

Figure 5. (a) Galvanometer mirror rotated in constant angular steps according to equation (8) producing the FPI output shown in (b). (c) Mirror rotated according to the arcosine angle function of equation (9) and resulting in the FPI output sampled in steps of constant phase shown in (d). The continuous curve in (d) is a cosine function fitted to the data. The FPI was a low finesse glass ($n_2 = 1.5$) cover slip of nominal thickness 150 μm.

low finesse. The single pass transfer function is therefore the familiar raised cosine function of a two beam interferometer and can be written as

$$I_R(\phi) = A + B\cos\phi(\theta) \tag{7}$$

where A and B are functions of the incident intensity and cavity mirror reflection coefficients and $\phi(\theta)$ is given by equation (6).

A linearly increasing voltage function generated by the PC was applied to the galvanometer mirror, thus rotating the optical beam in constant angular steps from normal incidence to a maximum angle $\theta_{\text{m}} = 11.2°$ according to

$$\theta = \theta_m \frac{i}{i_{\text{max}}} \tag{8}$$

where $i = 0, 1, 2, 3, \ldots, i_{\text{max}}$ and represents the index of

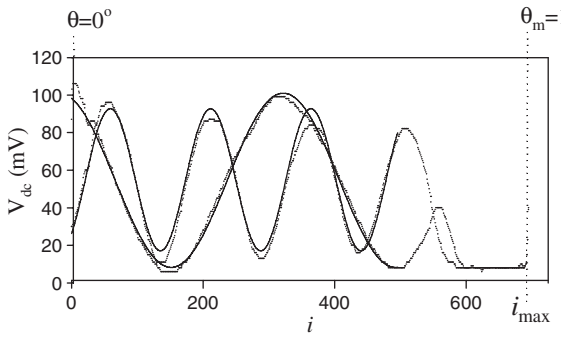

Figure 6. ITFs obtained using 50 and 125 μm thick low finesse PET ($n_2 = 1.65$) FPIs. The dotted curves represent the measured data. The continuous curves are cosine functions fitted to the data.

the array containing the voltage values that are sequentially applied to the mirror. This is shown in figure 5(a) along with the corresponding FPI output (represented by the photodiode voltage output V_{dc}) as a function of i in figure 5(b): the time taken to rotate the mirror and acquire this data was 0.5 s. The maxima and minima of the reflected fringes are clearly apparent in figure 5(b). However, they are not the equally spaced cosinusoidal fringes characteristic of a low finesse FPI due to the cosine angular dependence of the phase as defined by equation (6). As θ increases, the phase shift increases more rapidly causing the fringes to become increasingly bunched up.

To obtain the 'true' cosinusoidal ITF, the x-axis in figure 5(b) could be converted to a linear phase scale using equation (6). However, because I_R has been obtained in constant angular steps, the phase intervals at which the ITF is sampled would become progressively larger with increasing angle thus reducing the accuracy of the recovered ITF. It is more desirable to obtain I_R directly in steps of constant phase by applying an increasing arcosine voltage function to the galvanometer mirror of the form

$$\theta = \frac{n_2}{n_1}\cos^{-1}\left(1 - \frac{i}{i_{\max}}\left(1 - \cos\frac{n_1}{n_2}\theta_m\right)\right). \qquad (9)$$

This is shown in figure 5(c) along with the resulting transfer function in figure 5(d). The characteristic cosinusoidal shape of the ITF is now clearly apparent as confirmed by a cosine function fitted to the data—a good fit ($R^2 = 0.96$, where R^2 is the coefficient of determination) up to $i = 450$ ($\theta = 9°$) is obtained. Inserting $\lambda = 633$ nm, $n_1 = 1$, $n_2 = 1.5$ and $\theta_m = 11.2°$ into the phase term of the fitted cosine function and solving for l gives a value of $l = 162$ μm. Although reasonably close to the nominal cover slip thickness of 150 μm, it is difficult to assess the accuracy of the measurement on account of the manufacturer's large thickness tolerance. Further experimental data were therefore obtained using more tightly specified ($\pm$10% of the nominal thickness) PET (polyethylene terepthalate) films as FPIs. ITFs measured using 50 and 125 μm thick PET films ($n_2 = 1.65$) and their cosine fits are shown in figure 6: $R^2 = 0.99$ for the fit to the 50 μm PET film data and $R^2 = 0.98$ for the fit to the 125 μm PET film data. The values of l recovered from the fitted data are 56 and 124 μm, in good agreement with the known values. The closeness of the cosine fits to the experimental data in figures 5(d) and 6 and agreement of the recovered values of l with the known values of the PET FPIs indicates that, for $\theta < 9°$, $\theta = \theta_{in}$ and equation (6) is valid.

For $\theta > 9°$ ($i > 450$), discrepancies between the cosine fit and the experimental data are apparent in figure 5(d). This is most likely to be due to off-axis aberrations introduced by the lenses L1–3. The effect of such aberrations, particularly coma, is that a change in θ_{in} no longer results in an identical change in θ and the phase–angle relationship described by equation (6) is no longer directly applicable. At small angles the effect is negligible. At larger angles, as the beam moves further off-axis, the aberrations become more significant producing the distortion observed in the transfer function. Additionally, such aberrations will have the undesirable effect of translating the FPI input and output beams at P1 and P2 and thus adversely affecting the lateral spatial fidelity of the measurement. To minimize the deleterious effects of aberrations, it was found necessary to use achromatic doublets for L1–3.

The other potential source of ITF distortion is angle dependent transmission characteristics in the optical components of the system. However, the near-uniform amplitude of the fringes in figure 5 suggests this is negligible.

Two factors have not been accounted for. Firstly, the lateral beam walk-off that occurs as the angle of incidence increases. In principle this will reduce fringe visibility and the lateral spatial resolution of the measurement. However, for low finesse interferometers of less than a few hundred micron thickness, beam diameters greater than a few hundred microns and small angles ($\theta < 10°$), it can be neglected—it will be of greater significance for high finesse FPIs. Secondly, the area of the beam increases as $1/\cos\theta$ reducing the incident intensity and altering the geometry of the interrogated region. Again this is a marginal effect for small angles ($\theta < 10°$).

5. Sensor interrogation schemes

Two sensor interrogation methods have been investigated. The first (section 5.1) involves actively setting the phase bias of the FPI at its optimum point by scanning through the ITF and returning to the angle that corresponds to the peak value of the ITF phase derivative. The second (section 5.2) relies upon repetitively scanning through the ITF and capturing the signal as it naturally coincides in time with the peak value of the ITF phase derivative.

5.1. Active phase bias control

This method involves rotating the galvanometer mirror using the arcosine voltage function described by equation (9) and measuring the dc output of the photodiode V_{dc} to obtain the ITF in steps of constant phase as described in section 4. The derivative of the ITF is then calculated and the mirror returned to the angle that corresponds to the peak phase derivative, the point of maximum phase sensitivity. The system is then ready to make a measurement.

An automated control system based on this method was implemented in Labview (National Instruments). A typical system output obtained using a 40 μm thick FPI is shown in figure 7. This shows the ITF, V_{dc}, the corresponding derivative dV_{dc}/di and the optimal phase bias point ϕ_o located by the

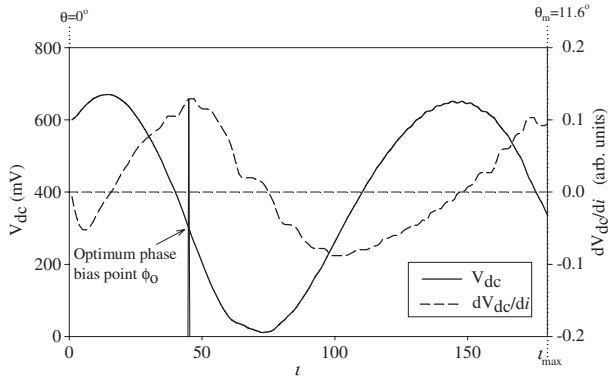

Figure 7. Output of active phase bias control system. The FPI is a 40 μm thick low finesse polymer film ($n_2 = 1.65$) FPI. The system rotates the mirror according to the arcosine function of equation (9) to obtain the ITF (represented by V_{dc}). The derivative dV_{dc}/di is computed and the mirror returned to the angle that corresponds to the peak value of dV_{dc}/di—the point of maximum sensitivity, indicated by the vertical line at $i = 48$.

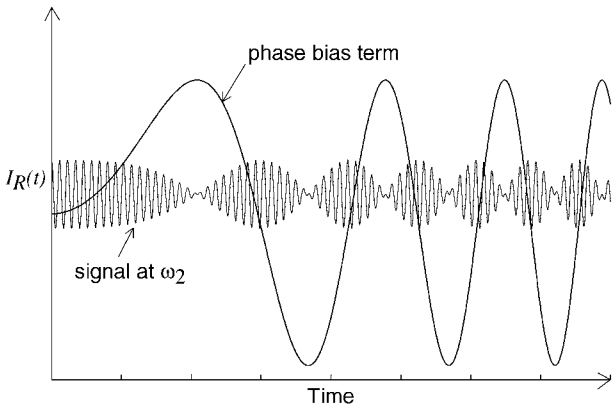

Figure 8. Simulation of phase bias term and signal term using a continuously rotating mirror to interrogate a low finesse FPI and applying a measurand varying sinusiodally at ω_2.

system. dV_{dc}/di provides a measure of the phase sensitivity. It can therefore be used to monitor variations in sensitivity. For example, if measurements at different points over an FP sensor are being made, sensitivity variations due to changes in intensity across the incident illuminating beam or variations in the FPI mirror reflectivities can be compensated for by dividing by the value of dV_{dc}/di obtained at ϕ_o—this also corrects for changes in the sign of the measurement should the system switch from locking on to a positive to a negative slope. This approach has successfully been used for mapping photoacoustic signals incident on a FP polymer film sensor [9].

5.2. Continuous phase bias scanning

An alternative to the 'search and locate' approach described above is to slowly and continuously modulate the phase bias over 2π radians and capture the signal at the instant in time it naturally coincides with the peak value of the ITF phase derivative. The advantage of this method is that it can be inexpensively implemented by replacing the PC controlled precision galvanometer in figure 4 with a mirror mounted on a dc motor that is continuously rotating through 360°. Assuming the mirror is rotating at constant angular frequency ω_1, the angle θ_{in} swept out across input lens L1 in figure 4 is a linear function in time t, thus

$$\theta_{in} = 2\omega_1 t. \tag{10}$$

Assume also a sinusoidally varying measurand that modulates the cavity thickness about its mean value l_o with amplitude dl at angular frequency ω_2. Thus the cavity thickness l becomes

$$l = l_o + dl\ \cos\omega_2 t. \tag{11}$$

Equations (10) (assuming $\theta = \theta_{in}$) and (11) are substituted into equation (6), to obtain the phase term. Assuming a low finesse FPI, equation (7) can then be used to write the time-dependent FPI output during the period the beam is sweeping across the input lens L1 as

$$I_R(t) = A + B\cos\left[\frac{4\pi n}{\lambda}(l_o + dl\cos\omega_2 t)\cos 2\omega_1 t\right]. \tag{12}$$

Expanding the phase term in (12) and assuming the rate at which the phase bias is scanned is much less than the measurand signal frequency, $2\omega_1 \ll \omega_2$, gives

$$I_R(t) = A + B\cos\underbrace{\left(\frac{4\pi n}{\lambda}l_o\cos 2\omega_1 t\right.}_{\phi_o(\omega_1)} + \underbrace{\left.\frac{4\pi n}{\lambda}dl\cos\omega_2 t\right)}_{d\phi(\omega_2)}. \tag{13}$$

Thus the phase term consists of two sinusoidally varying components. The first, $\phi_o(\omega_1)$ is due to the rotation of the mirror at $2\omega_1$ and represents the slowly varying phase bias. The second is the signal term $d\phi(\omega_2)$ at ω_2 and is due to the measurand induced thickness change. Making the substitutions for $\phi_o(\omega_1)$ and $d\phi(\omega_2)$

$$I_R(t) = A + B\cos(\phi_o(\omega_1) + d\phi(\omega_2)). \tag{14}$$

Expanding equation (14) and assuming $d\phi(\omega_2)$ is small so that $\sin d\phi = d\phi$ and $\cos\ d\phi = 1$ we get

$$I_R(t) = \underbrace{A + B\cos\phi_o(\omega_1)}_{\text{phase bias term}} - \underbrace{B\sin\phi_o(\omega_1)d\phi(\omega_2)}_{\text{signal term}}. \tag{15}$$

Thus the FPI intensity output can be separated into (i) a slowly varying phase bias term due to the angular variation at ω_1 and (ii) a signal term at ω_2 that is amplitude modulated by the phase bias variation as illustrated in figure 8. Equation (15) is recognizable as equation (1) with the low finesse ITF substituted for $I_R(\phi_o)$ and can be written more generally in terms of an arbitrary ITF and measurand-induced phase shift $d\phi(t)$

$$I_R(t) = I_R(\phi_o(\omega_1)) + I'_R(\phi_o(\omega_1))\,d\phi(t). \tag{16}$$

To demonstrate the concept, the 40 μm polymer film FPI used to obtain the data in figure 2 was positioned at P1 in figure 4. A mirror mounted on a dc motor, mounted in the back focal plane of L1 (in place of the galvanometer mirror) was used to angularly scan the beam over the aperture of the input lens L1. To create a repetitive signal term, short ultrasonic pulses at a repetition frequency of 10 kHz

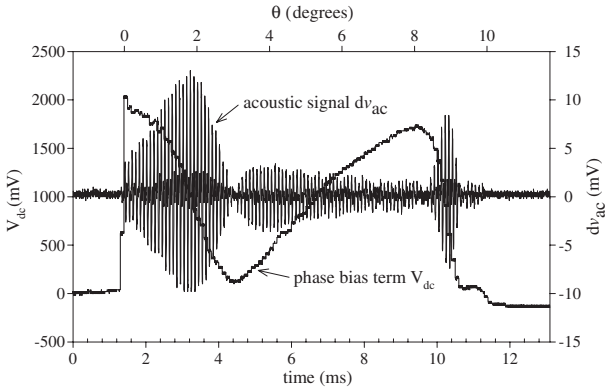

Figure 9. Output of a 40 μm polymer film FPI obtained by varying θ using a continuously rotating mirror (angular frequency $\omega_1 = 9$ rad s^{-1}) and applying ultrasonic pulses at a repetition frequency of 10 kHz ($\omega_2 = 6.28 \times 10^4$ rad s^{-1}), V_{dc} represents the slowly varying phase bias term due to the rotation of the mirror. $\mathrm{d}v_{\mathrm{ac}}$ represents the acoustically-induced signal term.

($\omega_2 = 6.28 \times 10^4$ rad s^{-1}), rather than a continuous sinusoidal variation, were used to modulate the optical thickness of the FPI. The angular frequency of the motor was 9 rad s^{-1} (1.43 Hz) and thus fulfilled the requirement that $2\omega_1 \ll \omega_2$. The output of the photodiode was connected to a 500 MHz DSO. This was triggered by a second photodiode positioned to detect the beam just prior to it sweeping across the aperture of lens L1. As the beam is slowly scanned over the lens aperture at a rate much less than the signal pulse repetition rate, the signal is captured at multiple points over the transfer function. By appropriate filtering, the time records of the phase bias V_{dc} and signal term $\mathrm{d}v_{\mathrm{ac}}$ were recovered separately and are displayed in figure 9. This shows similar behaviour to that depicted in figure 8 with the signal minima coinciding with turning points of the phase bias component. Note that unlike figure 8 however, the signal amplitude $\mathrm{d}v_{\mathrm{ac}}$ is lower when the slope of V_{dc} is positive compared to when it is negative. This is due to asymmetry in the intensity-phase ITF due to absorption in the aluminium coatings used to fabricate the mirrors of this particular FPI [8]: an indication of this asymmetry can be seen in the reflected interference fringes in figure 2(a) which were obtained using the same FPI. The derivative of the ITF and hence the phase sensitivity, and thus the signal amplitude, are therefore dependent upon the sign of the slope for this FPI. By contrast, an uncoated low finesse FPI is assumed for the simulation shown in figure 8. This has a cosinusoidal, and therefore symmetric, intensity-phase ITF and thus the signal amplitude is independent of the sign of the ITF slope.

One approach to recovering the signal is simply to convert the horizontal axis in figure 9, which is currently scaled in steps of constant angle, to a linear phase scale using equation (6). Subject to the sampling limitations discussed in section 4, this will provide the ITF. The peak value of the ITF derivative could then be calculated, and the acoustic signal corresponding to this point extracted from the time record of $\mathrm{d}v_{\mathrm{ac}}$.

If only the signal amplitude is required (rather than the temporal characteristics of the signal), a simpler approach can be adopted. That is to record only the signal $\mathrm{d}v_{\mathrm{ac}}$ over the duration the beam is being swept across input lens L1 and then apply a peak detect algorithm to the captured time record of $\mathrm{d}v_{\mathrm{ac}}$ in order to extract the maximum signal amplitude. This will automatically recover the amplitude of the signal coinciding with the point of maximum sensitivity. The advantage is that it is not necessary to attempt to recover the ITF shape, or indeed even record it. Distortion in the ITF, due to lens aberrations for example, are of little consequence. Providing $2\omega_1 \ll \omega_2$, the amplitude of the signal that coincides with the point of maximum phase sensitivity on the ITF will always be obtained. This approach has successfully been used to obtain 2D amplitude maps of ultrasound fields [10].

Assuming the $2\omega_1 \ll \omega_2$ requirement can be fulfilled, the principal advantage of the continuous scanning approach is that, by using a simple dc motor to vary θ, the expense of a precision galvanometer mirror and the closed loop PC control system is eliminated.

6. Conclusions

A practical and flexible method of interrogating free-space FP sensing interferometers by angle tuning has been described. This has shown that the ITF of low finesse FPI cavities of optical thicknesses down to 80 μm can be accurately recovered by tuning the external angle of incidence over less than 9°. Subject to the limitations imposed by off-axis lens aberrations discussed in section 4, higher numerical aperture lenses could be used to increase the angular excursion in order to interrogate shorter cavity thicknesses. Given the availability of high quality lenses of NA = 0.4, it should be possible to interrogate cavities down to approximately 10 μm in thickness. For large cavity thicknesses (>500 μm), where only a small angular excursion is required to obtain a 2π phase shift, the degradation in fringe visibility due to beam walk off rather than the effects of lens aberrations is likely to be the limiting factor.

There are several advantages of angle tuning over other methods of interrogating FP sensors. By dispensing with the need for a wavelength tunable source almost any fixed wavelength source of sufficient coherence can be used. Low cost He–Ne lasers or laser diodes can therefore be used. For mapping applications, high power sources can be used to illuminate a large area of the FPI with high intensity. Since angle tuning enables the phase bias to be varied continuously and rapidly using high speed resonant galvanometers (kHz) or electro-optic scanners (MHz) a variety of alternative signal processing methods can be used. For example, the phase could be modulated over 2π radians at a frequency several times higher than the highest signal frequency. The FPI output therefore becomes a high frequency carrier modulated in phase by the measurand [11] and recoverable using standard FM demodulation methods. Since the measurement is based on fringe shifts, it is independent, for example, of laser power fluctuations providing an inherently robust processing approach. Other robust processing methods that could be applied include a variety of phase stepping algorithms [12, 13] which could be implemented by illuminating sequentially or simultaneously at a range of discrete angles.

Acknowledgment

The author is supported by an EPSRC Advanced Fellowship.

References

[1] Singh H and Sirkis J S 1997 Simultaneously measuring temperature and strain using optical fibre microcavities *J. Lightwave Technol.* **15** 647–53

[2] Laufer J G, Beard P C, Walker S P and Mills T N 2001 Photothermal determination of optical coefficients of tissue phantoms using an optical fibre probe *Phys. Med. Biol.* **46** 2515–30

[3] Beard P C, Perennes F and Mills T N 1999 Transduction mechanisms of the Fabry–Perot polymer film sensing concept for wideband ultrasound detection *IEEE Trans. Ultrason. Ferroelectr. Freq. Control* **46** 1575–82

[4] Nakamura K and Nimura K 2000 Measurements of ultrasonic field and temperature by a fibre optic microprobe *J. Acoust. Soc. Japan* E **21** 267–9

[5] Wilkens V and Koch Ch 1999 Optical multilayer detection array for fast ultrasonic field mapping *Opt. Lett.* **24** 1026–8

[6] Beard P C and Mills T N 2000 An optical detection system for biomedical photoacoustic imaging *Proc. SPIE* **3916** 100–9

[7] Wilkens V 2003 Characterisation of an optical multilayer hydrophone with constant frequency response in the range 1–75 MHz *J. Acoust. Soc. Am.* **113** 1431–8

[8] Kilpatrick J M, MacPherson W N, Barton J S and Jones J D C 2000 Phase demodulation error of a fibre optic sensor with complex reflection coefficients *Appl. Opt.* **39** 1383–8

[9] Beard P C 2002 Photoacoustic imaging of blood vessel equivalent phantoms *Proc. SPIE* **4618** 54–62

[10] Beard P C and Mills T N 2000 A 2D optical ultrasound array using a polymer film sensing interferometer *IEEE Ultrason. Symp.* (Piscataway, NJ: IEEE) pp 1183–6

[11] Dandridge A 1991 Fiber optic sensors based on the Mach–Zender and Michelson interferometers *Fiber Optic Sensors: An Introduction for Engineers and Scientists* ed E Udd (Chichester: Wiley) pp 271–323 ISBN 0-471-83007-0

[12] MacPherson W N, Kidd S R, Barton J S and Jones J D C 1997 Phase demodulation in optical fibre Fabry–Perot sensors with inexact steps *IEE Proc.* J **144** 130–3

[13] Schmidt M, Werther B and Furstenau N 2001 Fiber-optic extrinsic Fabry–Perot interferometer strain sensor with $<$50 pm displacement resolution using three-wavelength digital phase demodulation *Opt. Express* **8** 475–80